Mesostructures

DOI: 10.1002/anie.200801755

Solving Complex Concentric Circular Mesostructures by Using Electron Tomography**

Pei Yuan, Nian Liu, Lingzhi Zhao, Xufeng Zhou, Liang Zhou, Graeme J. Auchterlonie, Xiangdong Yao, John Drennan, Gao Qing (Max) Lu, Jin Zou, and Chengzhong Yu**

In nature, ordered structures may present crystal symmetry and/or unconventional helical symmetry that can not be treated by traditional crystallography. The characterization of nanomaterials with helical symmetry creates an extraordinary challenge because of their complexity. The discovery of mesoporous materials[1] with versatile applications[2] has led nanoscience and nanotechnology research into a new dimension. Understanding the morphosynthesis, that is, the internal structure, the external morphology, and the formation mechanism of novel mesoporous materials is of scientific importance and technological necessity.[3] Recent developments have greatly increased the interest in helical mesostructures with chiral channels[4–7] and circular mesostructures[8–12] as a result of their unique morphologies and internal architectures. However, the determination and differentiation of a closed helical mesostructure with the pitch of several nanometers[9] from a concentric circular mesostructure[8,12] is a formidable challenge. Both the closed helical and concentric circular mesostructures cannot be solely described by traditional crystallography, such as by space groups and symmetry elements, and thus their mesostructures cannot be determined by either X-ray or electron diffraction.[13] Moreover, the structural difference between two mesostructures is very small (in the range of several nanometers) and is located more distinctly in the interior of the material. As a consequence, conventional transmission electron microscopy (TEM) cannot help in determining the hidden information and, in turn, solving the complex mesostructures.

Electron tomography (ET) is a rapidly developing technique that is used to obtain the reconstructed complex 3D structures from a tilt series of TEM images. Electron tomography was first used in biology[14–19] to understand cell organelles, subcellular aggregates, and whole cells. Recently, the technique has been increasingly applied in material science to study the morphology and structure of nanomaterials.[20–25] The inherent advantage of the ET technique should be helpful in solving mesostructures with complex symmetries.[5]

Herein, we demonstrate that, by using the state-of-the-art ET technique, the complex concentric circular (CC) hexagonal mesostructure can be successfully differentiated from its closed helical (CH) counterpart. The key step in our approach is to make use of each tomographic slice with a thickness of less than 1 nm so that the structural characteristics "hidden" in the interior of selected mesostructured objects can be captured. To our knowledge, this is the first report of using the ET method to solve a complex structure with both conventional crystal structures and unusual geometrical configurations.

The mesostructured silica employed in this study was synthesized by using octadecyltrimethyl ammonium bromide (C_{18}TAB) as a template and perfluorooctanoic acid (PFOA) as an additive (see the Supporting Information for details). A TEM image of a typical CC rod is shown in Figure 1 a. Hexagonal closely packed pore arrays can be clearly observed near the edges of the rod, which indicates that the pore channels are nearly perpendicular to the long axis of the rod. The distance between two adjacent pores (cell parameter, *a*) is 4.6 nm. For this selected rod, a series of tilted TEM images were digitally acquired along two orthogonal axes (see movies S1 and S2 in the Supporting Information). The morphology of the mesostructure does not change in the first tilting series (as shown clearly in movie S1 in the Supporting Information), while the ringlike pattern can be observed in the second tilting series (see movie S2 in the Supporting Information). These results indicate that the hexagonally patterned channels are wrapped circularly around the long axis of the rod.

To determine the nature of the channels along the axial direction, an ultramicrotome was employed to prepare thin sections (ca. 50 nm) for TEM observations. As shown in Figure 1 b, the cross-section of a rod is a circle and the pore channels are visible as concentric rings. It should be noted that, in conventional helical mesostructured rods where the

[*] P. Yuan, N. Liu, L. Zhao, X. Zhou, L. Zhou, Prof. C. Z. Yu
Department of Chemistry and
Shanghai Key Laboratory of Molecular Catalysis
and Innovative Materials
Fudan University, Shanghai, 200433 (China)
Fax: (+86) 21-6564-1740
E-mail: j.zou@uq.edu.au

P. Yuan, Prof. J. Zou
School of Engineering
University of Queensland
Queensland, QLD 4072 (Australia)
E-mail: czyu@fudan.edu.cn

G. J. Auchterlonie, Prof. J. Drennan, Prof. J. Zou
Centre for Microscopy and Microanalysis
University of Queensland, Queensland, QLD 4072 (Australia)

Dr. X. Yao, Prof. G. Q. Lu
ARC Centre of Excellence for Functional Nanomaterials
University of Queensland, Queensland, QLD 4072 (Australia)

[**] We thank the State Key Research Program (2004CB217804, 2006CB932302), the NSFC (20721063, 20573021), SLADP (B108), NCET, and the Australian Research Council for financial support. We thank Dr. Matthias Floetenmeyer (UQ) for help with the ultramicrotome experiments.

Supporting information for this article is available on the WWW under http://dx.doi.org/10.1002/anie.200801755.

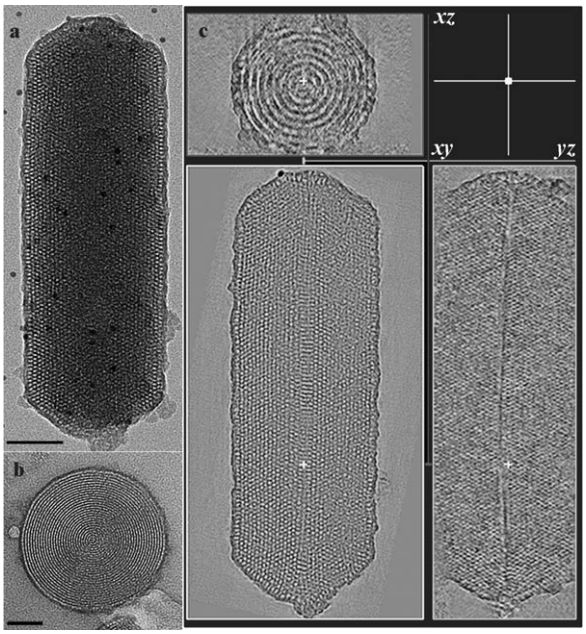

Figure 1. TEM images of: a) an individual CC rod (the black dots are 5 nm gold particles used for the alignment) and b) the cross-section of another CC rod prepared with the ultramicrotome. C) ET images viewed from three orthogonal directions of the rod shown in (a). The scale bar is 50 nm.

pitch (P) is relatively large (for example, >300 nm[4,6]), the thin section should have a hexagonal shape, with the dotlike pores arrayed hexagonally.[5] Based on this argument, the mesostructure shown in Figure 1b may be attributed to a CC rod or a CH rod with very small pitch, rather than a conventional helical rod.

To fully characterize the pore architectures, ET was carried out on the rod shown in Figure 1a. Figure 1c shows the bright-field ET images viewed from three orthogonal directions. From the ET image of the selected slice in the xz plane, eight concentric circular rings can be observed, and the diameter of this selected circular rod is approximately 128 nm. It is noted that the spacing between two adjacent circles is about 8.0 and 4.0 nm in the cross-section images obtained by ET (Figure 1c) and from the 2D projective TEM technique (Figure 1b), respectively. Such a difference between the ET and conventional TEM images recorded along the axial direction of the circular mesostructured rods has not been observed previously. Below we will demonstrate the origin of the difference and how to take advantage of the ET technique to solve the complex mesostructures.

In the ET processing, the thickness of each slice was artificially defined as 0.26 nm, thus about 18 slices can be obtained in the distance between two neighboring pores along the axial direction of the rod (4.6 nm). Therefore, even for a helix with the smallest pitch P (ca. 4.6 nm), the ET technique can still unambiguously provide "local information" to distinguish between a CC and CH mesostructure. In contrast, for the sample shown in Figure 1b, the thickness of the ultramicrotomed specimen is approximately 50 nm, so that the TEM contrast reflects the "projected information" of tens of complex pore structures overlapped in the depth of the specimen. The different circle-to-circle distance mentioned earlier can thus be explained by the difference between the ET and TEM techniques.

Theoretically, there are two possible ordered pore configurations. The [10] direction (indicated by red arrows in Figure 2a,b) of the 2D hexagonally arrayed pore channels

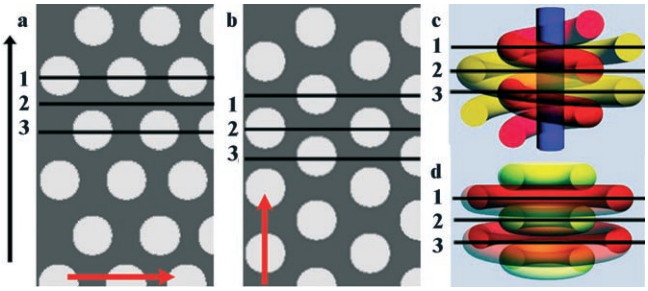

Figure 2. Schematic models of hexagonally arrayed pore channels when the [10] direction (indicated by the red arrows) and the long axis of the rod (shown by the black arrow) are: a) perpendicular and b) parallel; the 3D pore channels in the: c) CH ($P=a$, 4.6 nm) and d) CC structure from model (b) is determined. The number 1, 2, and 3 indicates selected slices while the spacing between two adjacent slices is $\sqrt{3}a/4$ in (a) and $0.5\,a$ in (b–d).

can be either perpendicular (Figure 2a) or parallel (Figure 2b) to the long axis of the rod (shown by the black arrow). The perpendicular model can be directly ruled out from the direct observation of the TEM image at the edge of the rod (Figure 1a) and from the ET studies. The ET images can show the projections in the xz plane (Figure 1c) at a selected height along the y-axis, as marked by 1, 2, and 3 in Figure 2a,b. For the parallel model (Figure 2b), projections 1, 2, and 3 should reflect the same (11) plane albeit from planes 1 to 2, and the pore and the wall will exchange their positions. In addition, the distance between two adjacent circles in the ET images and in the cross-section TEM images should be $\sqrt{3}a$ (8.0 nm) and $\sqrt{3}a/2$, respectively, which is in excellent agreement with our experimental observations.

The 3D models of the CH and CC pore channels with the [10] direction parallel to the long axis of the rod are represented in Figure 2c,d, respectively. The difference between these two structures can now be distinguished by the slices located in planes 1, 2 and 3. Figure 3a–c shows the ET images of three slices along the y-axis and the spacing between two adjacent slices is $0.5\,a$ (in accordance with the models shown in Figure 2c,d). The difference in the center of the white rings (reflecting the pores) can be clearly seen from the three images. A relatively larger, then smaller, and then larger white ring can be clearly distinguished on going from Figure 3a to 3b and then to 3c. Moreover, the locations of the white and black rings (reflecting the silica walls) in Figure 3a are now replaced by black and white rings when the slice is moved by $0.5\,a$ along the y-axis (Figure 3b). Some irregular contrast reversals are observed in Figure 3a–c which can be attributed to the defects existing in the material (see the Supporting Information). Such detailed experimental observations are in good agreement with the simulated images for a CC structure (Figure 3d–f) obtained in planes 1–3 indicated

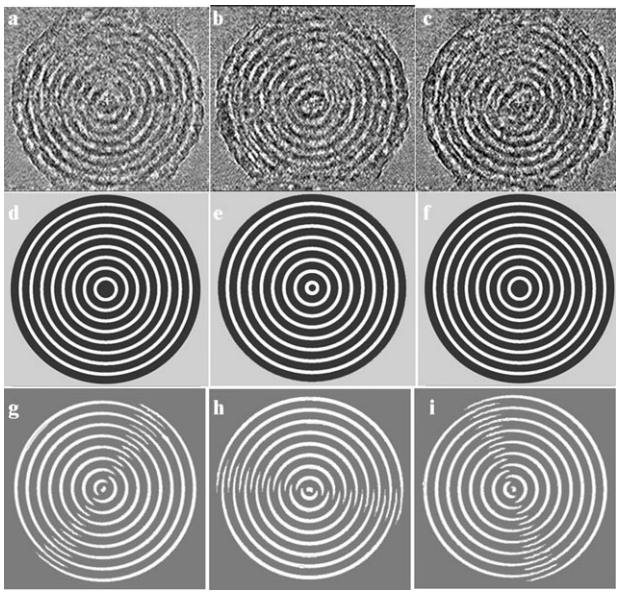

Figure 3. ET images of three slices (a–c) along the *y*-axis. The spacing between two adjacent slices is 0.5 *a*. Simulated images (d–f) from a CC structure obtained at planes 1, 2, 3 as shown in Figure 2 d. Simulated images (g–i) from a CH structure obtained at planes 1, 2, 3 shown in Figure 2 c.

in Figure 2 d. For comparison, the simulated images based on the CH structure with pitch *a* do not show the same change in the shape of these most inner rings (Figure 3 g–i). Instead, a fanlike fringe appears that rotates as the position on the *y*-axis is changed; this finding is different to our results. On the basis of these results, the possibility of the sample having a CH structure with the smallest possible pitch can now be unequivocally excluded.

Indeed, as shown in Figure 2 c, d, the most distinct structural features that differentiate the CC and CH mesostructures are located in the center of the rod. This significant information cannot be observed in conventional TEM images (for example, Figure 1 a) because of the overlapping thickness effect. In contrast, the advantage of ET over conventional TEM techniques may reveal such "hidden" information. The CC mesostructure can be further clarified by the ET images recorded in the *xy* plane at different *z* positions (Figure 4 a–c). The slice shown in Figure 4 a is obtained when the *xy* plane is very close to the center of the rod. The black and white stripes are parallel to each other, but perpendicular to the long axis of the rod. This is also the case for the ET images obtained in the *xy* plane but which are far from the center (ca. 33 and 60 nm for Figure 4 b, c, respectively). Such information is consistent with the simulated image obtained from a CC mesostructure in the *xy* plane (Figure 4 d). It is also notable that there exists an enantiomorphic plane in Figure 4 a (in the middle and along the long axis of the rod), in accordance with Figure 2 d and the CC mesostructure.[12]

It should be noted that the CH model shown in Figure 2 c is based on a close-packed helix with $P = a$. The resultant structure pattern needs to be be further examined for a CH mesostructure where P is larger than a. The simulated image for a CH mesostructure with a pitch of $3a$ (ca. 13.8 nm) is

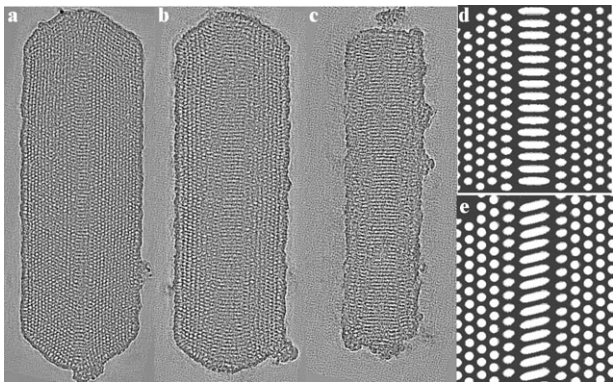

Figure 4. ET images in the *xy* plane at different *z* positions (a–c) when the deviation from the center of the circular circle is about 7, 33, 60 nm, respectively. Simulated images from the CC (d) and CH (e) structure.

shown in Figure 4 e. The black and white stripes are still parallel to each other, but no longer perpendicular to the long axis of the rod. This deviation is a function of P and will increase as P is enlarged. From the comparison between this model and Figure 4 a–c, the CH mesostructure can now be exclusively ruled out and the CC mesostructure further confirmed.

In conclusion, the true internal structure of the concentric circular hexagonal mesostructure has been solved for the first time by using electron tomography. This is a significant step forward in solving such complex mesostructures and paves the way for understanding the origins of the CC mesostructure and the evolution of conventional helical to CC structures. It is believed that this method can be further extended to solve other complex structures with unconventional symmetries and configurations.

Experimental Section

All chemicals were used as received without further purification. C_{18}TAB and PFOA were purchased from Aldrich. Other chemicals were purchased from the Shanghai Chemical Company. The mesostructured material was synthesized under basic conditions by using C_{18}TAB as a template and PFOA as an additive. ET was performed with a FEI Tecnai F30 electron microscope operating at 300 kV. All TEM images were recorded at a given defocus in a bright-field mode to show the thickness contrast. Alignment and three-dimensional reconstructions of concentric circular structures by filtered back projection were performed with IMOD software.[26] Details can be found in the Supporting Information. It is noted that all the products have a hexagonal structure, but are CC rods and conventional helical rods ($P > 300$ nm). The helical rods are similar to those formed by the cetyltrimethyl ammonium bromide (CTAB)/PFOA templating technique.[6] In this study, we focused only on the unambiguous identification of the CC mesostructure. The XRD and N_2 sorption analysis results can be found in the Supporting Information.

Received: April 15, 2008
Published online: July 22, 2008

Keywords: electron tomography · mesostructures · self-assembly · structure elucidation · transmission electron microscopy

[1] C. T. Kresge, M. E. Leonowicz, W. J. Roth, J. C. Vartuli, J. S. Beck, *Nature* **1992**, *359*, 710.
[2] M. E. Davis, *Nature* **2002**, *417*, 813.
[3] H. Yang, N. Coombs, G. A. Ozin, *Nature* **1997**, *386*, 692.
[4] S. Che, Z. Liu, T. Ohsuna, K. Sakamoto, O. Terasaki, T. Tatsumi, *Nature* **2004**, *429*, 281.
[5] T. Ohsuna, Z. Liu, S. N. Che, O. Terasaki, *Small* **2005**, *1*, 233.
[6] S. Yang, L. Z. Zhao, C. Z. Yu, X. F. Zhou, J. W. Tang, P. Yuan, D. Y. Chen, D. Y. Zhao, *J. Am. Chem. Soc.* **2006**, *128*, 10460.
[7] Y. Han, L. Zhao, J. Y. Ying, *Adv. Mater.* **2007**, *19*, 2454.
[8] J. F. Wang, C. K. Tsung, W. B. Hong, Y. Y. Wu, J. Tang, G. D. Stucky, *Chem. Mater.* **2004**, *16*, 5169.
[9] F. Marlow, A. S. G. Khalila, M. Stempniewicz, *J. Mater. Chem.* **2007**, *17*, 2168.
[10] F. Marlow, B. Spliethoff, B. Tesche, D. Y. Zhao, *Adv. Mater.* **2000**, *12*, 961.
[11] F. Kleitz, F. Marlow, G. D. Stucky, F. Schuth, *Chem. Mater.* **2001**, *13*, 3587.
[12] Y. Y. Wu, G. S. Cheng, K. Katsov, S. W. Sides, J. F. Wang, J. Tang, G. H. Fredrickson, M. Moskovits, G. D. Stucky, *Nat. Mater.* **2004**, *3*, 816.
[13] Y. Sakamoto, M. Kaneda, O. Terasaki, D. Y. Zhao, J. M. Kim, G. Stucky, H. J. Shim, R. Ryoo, *Nature* **2000**, *408*, 449.
[14] H. X. Sui, K. H. Downing, *Nature* **2006**, *442*, 475.
[15] D. Nicastro, C. Schwartz, J. Pierson, R. Gaudette, M. E. Porter, J. R. McIntosh, *Science* **2006**, *313*, 944.
[16] M. Beck, F. Forster, M. Ecke, J. M. Plitzko, F. Melchior, G. Gerisch, W. Baumeister, O. Medalia, *Science* **2004**, *306*, 1387.
[17] M. Beck, V. Lucic, F. Forster, W. Baumeister, O. Medalia, *Nature* **2007**, *449*, 611.
[18] J. Kurner, A. S. Frangakis, W. Baumeister, *Science* **2005**, *307*, 436.
[19] J. Liu, D. W. Taylor, E. B. Krementsova, K. M. Trybus, K. A. Taylor, *Nature* **2006**, *442*, 208.
[20] P. A. Midgley, E. P. W. Ward, A. B. Hungria, J. M. Thomas, *Chem. Soc. Rev.* **2007**, *36*, 1477.
[21] H. S. Kim, S. O. Hwang, Y. Myung, J. Park, S. Y. Bae, J. P. Ahn, *Nano Lett.* **2008**, *8*, 551.
[22] K. Kaneko, K. Inoke, B. Freitag, A. B. Hungria, P. A. Midgley, T. W. Hansen, J. Zhang, S. Ohara, T. Adschiri, *Nano Lett.* **2007**, *7*, 421.
[23] I. Arslan, T. J. V. Yates, N. D. Browning, P. A. Midgley, *Science* **2005**, *309*, 2195.
[24] H. Friedrich, J. R. A. Sietsma, P. E. de Jongh, A. J. Verkleij, K. P. de Jong, *J. Am. Chem. Soc.* **2007**, *129*, 10249.
[25] T. J. V. Yates, J. M. Thomas, J. J. Fernandez, O. Terasaki, R. Ryoo, P. A. Midgley, *Chem. Phys. Lett.* **2006**, *418*, 540.
[26] J. R. Kremer, D. N. Mastronarde, J. R. McIntosh, *J. Struct. Biol.* **1996**, *116*, 71.

